Multi-kernel deconvolution applied to confocal fluorescence microscopy with engineered point spread function

Bertrand Simon, Olivier Haeberlé

Multi-kernel deconvolution applied to confocal fluorescence microscopy with engineered point spread function

Bertrand Simon and Olivier Haeberlé

Laboratoire MIPS - Groupe Lab.El, Université de Haute-Alsace

IUT Mulhouse, 61 rue A. Camus F-68093 Mulhouse Cedex France

bertrand.simon@uha.fr olivier.haeberle@uha.fr

Fluorescence microscopy is a powerful technique in biology, because of the immense variety of markers now available. Compared to other methods, its resolution is however limited. In wide-field microscopy, the technique of structured illumination permits to improve the lateral resolution by a factor of two, even surpassing confocal microscopy, which permits a theoretical gain of about 40%. We propose an alternate technique, combining laterally interfering focused beams, which should permit the same gain of resolution in a confocal microscope. Furthermore, this technique, combined with multiple acquisition and multikernel deconvolution, permits a better object reconstruction than classical monokernel deconvolution using a regular excitation point spread function.

Keywords: point spread function engineering, multi-kernel deconvolution, confocal fluorescence microscopy.

1. Introduction

At the end of 19th century, Ernst Abbe [1] introduced for conventional microscopy his resolution criterion as:

$$R_{Abbe} = 0.5\lambda/NA \,, \tag{1}$$

with λ being the wavelength of observation and NA being the numerical aperture of the objective, defined as $NA = n \sin\alpha$. In this formula, n represents the index of refraction of the observation medium, and α is the maximum angle of collection of the objective. The Abbe resolution criterion is in fact nothing else than the Full Width at Half Maximum (FWHM) of the detection Point Spread Function (PSF) of the objective, calculated using the scalar approximation of diffraction. For decades, the resolution limit was explained by the Abbe formula. However, the Abbe limit assumes that all points of an object emit light in the same manner.

One had to wait the invention of the confocal microscope by Marvin Minski [2] to get a first breakthrough. In a confocal microscope, the specimen is not anymore uniformly illuminated, but using a focalized beam, and a detection pinhole cutting most of the out-of-focus light.

A probabilistic interpretation of the detection process gives a simple explanation of the improved resolution in confocal microscopy. In a wide-field microscope, the probability for a photon to reach the detector is given by the product of the probability of the photon to be created (equal to one, because of the uniform excitation) by the probability for the photon to be detected P_d, which is described by the detection PSF_{det}. In a confocal microscope, the probability of excitation P_e is modeled by the excitation PSF_{exc}, so that the confocal PSF is in first approximation simply given by multiplying the illumination PSF_{ill} by the detection PSF_{det} (the detection PSF_{det} being even wider because of the Stokes shift). Multiplying both PSFs leads to a lateral resolution improvement of about 40%, for an infinitely small pinhole. However in practice, in order to efficiently collect fluorescence photons, one must open the pinhole to a size similar to the Airy disk. As a consequence, the gain in lateral resolution is usually much smaller, the main interest of the confocal setup being its better optical sectioning capabilities, compared to a wide field microscope.

Mats Gustafsson has proposed [3,4] another technique called structured illumination, which permits to improve the lateral resolution by a factor of two in a wide field microscope, so even beating confocal microscopy. Confocal microscopy may in fact also be considered as a structured illumination technique,

the illumination being reduced to a focalized excitation spot. Structured illumination however is a wide-field technique using a sinusoidally modulated excitation, and does not require a detection pinhole. As a consequence, it also has the advantage (compared to confocal microscopy) that no emitted fluorescence is discarded. Structured illumination however requires taking several images of the same specimen (typically 7 to 9 for two dimensional imaging [3]) to recompose a resolution-improved image, which may be a drawback for bleaching-sensitive dyes.

The aim of this work is to show how the same gain of a factor of two in lateral resolution (compared to Abbe's limit) may be obtained in a confocal microscope, with a technique using three laterally interfering excitation PSF_{ill} in order to decrease the spatial extension of the total PSF along one spatial direction, and a recombination of typically four images of the same sample, observed with different orientations of the narrowed PSF.

2. Structured illumination in fluorescence microscopy

Several techniques to use structured illumination in fluorescence microscopy have been proposed in the literature. We here briefly recall them, in order to highlight their common features and differences.

2.1 Axially structured illumination: wide-field interfering beams

In a standing wave fluorescence microscope, the excitation consists of two counter propagating plane waves, which form by interference a standing wave [5,6]. The axial modulation produces a Moiré pattern, which mixes axial high space frequencies (normally lost into the so-called "missing cone") into the limited set of special frequencies one can usually acquire with a given objective. In order to demodulate this mixed information, one must acquire three different images with different phases of the standing wave [5,6]. However, a set of intermediate frequency is not mixed into the observation space by the Moiré effect, which makes 3-D reconstructions problematic in some cases [7,8].

A variant of standing wave illumination is the so-called I^3M or incoherent interference illumination microscopy [9], which uses two opposing objectives in order to focus illumination light. It is also a wide-field technique, and provides better axial sectioning capabilities than standing wave microscopy. However, I^3M still presents missing frequencies along the optical axis [8].

2.2 Axially structured illumination: focused interfering beams

An alternate to I^3M is to use a coherent, focused illumination from two opposing objective, in a configuration called 4Pi microscopy of type A [10]. In order to improve the imaging capabilities of the 4Pi microscope of type A, one usually couples the 4PiA illumination scheme with a coherent detection of the fluorescence through both opposing objectives (4Pi type B) in a configuration called 4Pi type C [11].

The main advantage of 4Pi microscopies is that being scanning techniques, the reconstruction of the observed object is straightforward, the remaining side lobes being removed by a simple inverse filtering technique [12]. Being a scanning technique, it may however be slower than wide-field techniques like I^3M.

The most noticeable feature to be remembered is that these optical set-ups (I^3M, 4Pi) do not in fact provide a gain in lateral resolution compared to a regular confocal microscope when used at its optimum.

2.3 Laterally structured illumination: wide-field interfering beams

It is also possible to improve the lateral resolution in wide-field microscopy by the technique of structured illumination, using two interfering illumination beams [13] or with a diffraction grating [14]. In this technique, a Moiré effect is used to code normally undetected information, carried by high frequency spatial components, into the detectable region of spatial frequencies. As for standing wave or I^3M, one has to take several images of the specimen in order to decode the information. The technique has been demonstrated in 2-D, and it has been shown that the lateral resolution limit (Abbe criterion) can be surpassed by a factor of two [3,4].

The main advantage of this technique is that no light is discarded by a pinhole, so that it is very efficient. Being a wide-field technique, it also permits fast acquisition. The mathematical processing of the images is also fast compared to deconvolution techniques. However, in order to obtain a gain in resolution in all direction, typically 9 images of the same specimen of the specimen must be taken and processed [3]. Similarly, a 2-D spatial modulation may be used [15].

2.4 Laterally structured illumination: focused interfering beams

In Ref. [16], we have described various schemes, which permit to decrease the lateral extension of the illumination PSF_{ill} in a confocal microscope. We here briefly recall the main points of a technique, which

is, compared to laterally structured illumination with wide-field interfering beams what 4PiA is, compared to I^3M, to axially structured illumination.

We consider for computing PSF_{ill} the vectorial model of Haeberlé, as described in Refs. [17-19]. The detection PSF_{det} is computed using the vectorial dipole model of Haeberlé *et al*. [20,21]. When using a x-polarized incident beam, the three components of the electromagnetic field at point P(x,y,z) in the specimen are given by (with ϕ_p in spherical polar coordinates):

$$E_x = -i(I_{0ill} + I_{2ill}\cos 2\phi_p)\ ,\ E_y = -i(I_{2ill}\sin 2\phi_p)\ ,\ E_z = -2I_{1ill}\cos\phi_p\ . \qquad (2)$$

A detailed description of how to compute the three diffraction integrals I_0, I_1 and I_2, is given in Refs. [17-22].

Figure 1 describes the considered configuration, with three x-polarized incident beams giving rise to three PSF_{ill} slightly shifted along the y-axis. As explained in Ref. [16], a substantial narrowing of the central Airy disk may be obtained by properly shifting and dephasing both lateral spot.

Figure 2 shows the computational results for an illumination wavelength λ_{ill} = 400 nm, using a special NA=1.65 objective combined with a special preparation of the 2-D sample, as explained in Ref. [16]. Figure 2(a) shows the illumination PSF_{ill} for a "regular" confocal microscope with x-polarized illumination. Figure 2(b) shows the corresponding confocal PSF, modeled by the product of the illumination PSF_{ill} and the detection PSF_{det}, when observing at λ_{det} = 500 nm (for example considering the Bis-ANS (B153) tubulin from Molecular Probes). The detection PSF_{det} is computed considering random polarization emission.

Figure 2(c) shows the PSF_{ill} computed using the three-beam illumination scheme we propose. The central spot is much narrower than the spot on Fig. 2(a), as expected, but the presence of two strong lateral lobes renders confocalization mandatory to suppress them (see Figure 2(d)).

It is important to note that with this three-beam illumination configuration, the confocalization process does not significantly improve the resolution along the y-axis, as illustrated by Figure 3, which shows PSF_{ill}, PSF_{det} and PSF_{conf} computed for a more conventional NA=1.2 water immersion objective, considering λ_{ill} = 400 nm and λ_{det} = 500 nm, and using a standard (170 μm thickness, n=1.525) cover glass, and imaging into a watery specimen. The central spot of PSF_{ill} has a y-width of 104 nm while the Abbe criterion gives 208 nm for this configuration. This shows that a factor two in resolution can be

expected from a confocal microscope, compared to the Abbe limit, using a structured point spread function. This is the same factor two that was already demonstrated in classical fluorescence microscopy using a wide-field structured illumination [3]. Confocalizing then only marginally improves the resolution, and PSF_{conf} has a FWHM of 100 nm. The remaining side-lobes may induce the apparition of ghost images surrounding the main image, as for example in 4Pi-confocal microscopy [10]. It has however been shown that fast linear filtering is sufficient to effectively remove these ghost images [12].

However, with this three-beam illumination scheme, the asymmetry of PSF_{conf} remains important, as can be noticed on Fig. 2(d). As a consequence, images acquired with such a structured PSF_{ill} will present an optimally improved resolution along the y-axis only, which is unfavorable in practice. Only for 1-D specimens, like for example DNA fragments or microtubules deposited on a glass slide could such a mono-axis gain in resolution be really helpful.

We show in the next section how the combination of several images improved along one different axis each may permit to obtain a true 2-D resolution improvement, and apply the image processing approach we propose to this later case of confocal PSF engineering.

3. Image processing: multikernel deconvolution

In the previous section, we have shown the possibility to improve the lateral resolution in confocal fluorescence microscopy using an interfering three-beam illumination. We have seen that the gain in resolution is up to a factor of two, but along one direction only. One may however take several images of the same specimen, with improved resolution along different directions. Data fusion techniques can then be used to recombine these images in order to benefit from the resolution enhancement along all spatial directions. Another approach is deconvolution. One may first deconvolve individually each image, and then recombine them. We propose to use a combined approach, called multi-kernel deconvolution.

Each recorded image I(X) can be described by the following convolution equation:

$$I(X) = \int_{-\infty}^{+\infty} H(X - X_1)O(X_1)dX_1 \oplus b(X) \tag{3}$$

where X and X_1 are 3-D coordinates, H(X) describes the Point Spread Function (PSF) of the acquisition system and O(X) is the original object. The term b(X) represents a combination of noise sources due to the fluorescence process and the acquisition electronics. In the frequency domain this

equation can be rewritten as:

$$\hat{I}(\omega_x,\omega_y) = \hat{O}(\omega_x,\omega_y) \times \hat{H}(\omega_x,\omega_y) + \hat{b}(\omega_x,\omega_y) \ . \quad (4)$$

In the frequency domain, the Optical Transfer Function (OTF) $\hat{H}$ behaves as a filter, which only partly transmits the object spatial frequencies. The resolution improvement along the y-axis when using a three-beam confocal PSF can be interpreted as a better transmission of higher frequencies along this axis by the microscope. Better transmission means that the support of the transmitted frequencies is larger (because of the confocalization effect when comparing to a wide-field microscope), and within this extended support, the attenuation of higher frequencies is lower when using a three-beam illumination than when using a regular confocal illumination. Making several acquisitions with different orientations of the three-beam illumination will result in several images showing differently orientated enhanced details.

Figure 4 illustrates this behaviour with simulations. In this section, all computations are performed considering a NA=1.2 water immersion objective, with λ_{ill} = 400 nm and λ_{det} = 500 nm. The object O represents the famous Abbe formula (Fig. 4(a)). Figures 4(b-d) represent three-beam confocal PSFs from interfering beams linearly polarized at θ=0°, 45° and 90° with respect to the x-axis, respectively, and computed with same parameters as for Fig. 3. Figures 4(e-g) display the corresponding simulated images. Note for example, that in Figs. 4(f) and 4(g) the fraction bar is not visible, while it is clearly noticeable in Fig. 4(e). Typically this is because this fraction bar represents an almost 1-D object barely oriented along the x-axis. As a consequence, to detect it, one must have good resolution along the y-axis, which is indeed obtained when using x-polarized beams, while y-polarized beams (θ=90°) permit a better resolution along the x-axis, so that vertical details are more noticeable, as for example the letter λ is more visible in Fig. 4(g) than in Fig. 4(e).

In order to simultaneously deconvolve several images keeping the best of each, Ghiglia [23] proposed a multikernel deconvolution approach. This technique permits to take into account the diversity of information obtained during the acquisition of a series of image of a same object with several transfer functions. More over, it makes it possible to be released from an important constraint of the deconvolution process related to the fact that the transfer function of an imaging system contains zeros, which implies the loss of certain object spatial frequencies. Indeed, in our case, each transfer function

presents zeros, which are located in different directions, and a part of the frequencies lost in one image is theoretically recoverable from another image.

Goudail *et al* [24] studied multikernel deconvolution with the aim of quantifying the efficiency and the robustness of such a technique. They adapted a Thikonov regularized deconvolution filter to the multikernel deconvolution problem. We propose to use their approach in the case of the laterally compressed PSF. We consider the acquisition of a series of k images of a same scene O convolved by the k kernels resulting from k successive rotations of the direction of polarization of the three-beam excitation PSF. Reeves *et al*. [25] write the classical Thikonov regularized deconvolution operator as:

$$\hat{O}'(\omega_x,\omega_y) = \frac{\sum_{k=1}^{n} \hat{H}_k(\omega_x,\omega_y) \times \hat{I}_k(\omega_x,\omega_y)}{\sum_{k=1}^{n} \left|\hat{H}_k(\omega_x,\omega_y)\right|^2 + \lambda \left|L(\omega_x,\omega_y)\right|^2}, \tag{5}$$

where $\hat{O}'$ represents the estimated Fourier transform of the object, L is the transfer function of a classical Laplacian filter, and λ is a scalar variable that makes it possible to balance the effect of L, $\hat{H}_k$ and $\hat{I}_k$ being the successive OTFs (or kernels) and images, respectively.

We applied this multikernel deconvolution method on different series of numerically simulated images. Figure 5 shows the same binary object than Figure 4, whose acquisitions have been simulated for n=2 and θ=0° and 90°, n=4 and θ=0°, 45°, 90° and 135°, and finally for n=8 in steps of 22.5°. The results of the multikernel deconvolution are shown on Figs. 5(b) to 5(d), respectively. Note that if, as expected, a large number of acquisitions (8 for Fig. 5(d)) permits an excellent reconstruction of the original object, even with only four different acquisitions, one can perfectly recognize the original formula in Fig. 5(c). It is indeed important in practice to keep the mandatory number of acquisitions as low as possible, because of photobleaching effects, induced phototoxicity, or simply speed of acquisition for live specimens, which may slightly move over a long period of observation. If a priori information about the specimen is given, for example the orientation of fibres, DNA fragment or microtubules, one may choose the polarization orientation so as to minimize the number of acquisitions by orienting the PSF along the directions of the significant spatial frequencies needed to properly reconstruct the object.

Another important limiting parameter for image deconvolution is noise. Indeed, catastrophic amplification of noise may occur, which may render the deconvolution result useless. An important point in order to get optimal results is to determine the optimal level of regularization of the deconvolution

process with respect to the noise present in the image [26].

The case of multikernel deconvolution is slightly more favourable. Indeed, it can be considered that each image of the series is perturbed by an independent noise realization. Goudail *et al.*[24] studied the advantage of the multikernel approach with respect to the robustness to noise in the case of two-kernel deconvolution. Their conclusions highlight the positive effect of noise averaging permitted by this approach: because the algorithm is based on the addition of several processed images (see Eq. (5)). As a consequence, one may expect an increase of the robustness of the inversion process with respect to the noise by taking a larger number of images with different kernels. So the benefit of multikernel deconvolution with narrowed PSFs is double, permitting not only a better final resolution by combining several views of the same specimen, but also a lower sensitivity to noise.

In Figs. 6(b)-(d) we show the simulation of acquisitions of Fig. 6(a) taken with different signal to noise ratios, respectively no noise, 20 db and 3 dB SNR and for a three-beam-excitation confocal kernel oriented at θ=90°. Figs. 6(e)-(g) show the results of 4-kernel deconvolutions, based on 4-image series acquired with kernels oriented at θ=0°, 45°, 90° and 135°, and with no noise, 20 db and 3 dB SNR respectively. For comparison, Figs. 6(h)-(j) show the results of monokernel deconvolutions of the simulated images, which would have been obtained for a conventional x-polarized confocal PSF with same noise ratios.

To perform these monokernel deconvolutions, one simply uses Eq. (5) with n=1. In order to provide a fair comparison, Figs. 6(h)-(j) are obtained averaging 4 monokernel deconvolutions, in order to minimize the effect of noise, as the multikernel algorithm does.

In each case, the result of a 4-kernel deconvolution is of higher quality than that based on monokernel deconvolution. While not always clearly visible by eye (a thorough examination shows that Fig. 6(i) obtained for 20 dB SNR of noise monokernel deconvolution has similar quality than Fig. 6(g), obtained with multikernel deconvolution, but for a 3 dB SNR), the use of a quantitative measurement between the original object and the reconstructed one clearly shows this property of multikernel deconvolution. In order to highlight these better restoration capabilities of multikernel deconvolution combined with narrowed three-beam PSF_{conf} acquisitions compared to monokernel deconvolution with regular PSF_{conf} acquisitions, we show on Fig. 7 the quadratic error computed between the original and the restored objects, and plotted as a function of the filtering parameter λ, for 4-kernel deconvolutions (solid line) and

for monokernel deconvolutions (dashed line), with a SNR of 20 dB (Fig. 7(a)) and 3 dB (Fig. 7(b)). The results presented on Fig. 6 indeed correspond to optimal deconvolutions obtained at the minimum of these curves.

The optimal level for the filtering parameter λ is different for each case, but the quadratic error at the optimum is lower, for both levels of noise, when considering 4-kernel deconvolution compared to monokernel deconvolution (Same conclusion holds when considering multi- and monokernel deconvolutions without noise in the images).

Furthermore, the quadratic error for multikernel deconvolution is lower than the absolute minimum for monokernel deconvolution, and this over a large range for the filtering parameter λ (as shown by the dotted rectangles), showing that multikernel deconvolution, even if not performed at its best, gives better results than monokernel deconvolution. This may be of importance in practical cases, because biologists are often not specialists of image processing techniques, but multikernel deconvolution would then offer a supplemental margin of error in the choice the filtering parameter. The results we obtain confirm in the case of asymmetric PSFs those obtained by Goudail *et al*. [24] who considered multikernel deconvolution with symmetric PSFs, but of different sizes.

Another important property of multikernel deconvolution, which was enlighten by Goudail *et al*. [24] is the robustness of this technique with respect to the exact knowledge of the PSFs, which are used for deconvolution. In our case, taking several images of the sample would require a precise rotation of this sample. We studied the effect of angular errors, which may affect the actual angular positions of the sample with respect to the ideal ones, in the case of 4-kernel deconvolutions, wich are supposed to be taken at angle 0°, 45°, 90° and 135°, respectively. We have applied a systematic angular shift to the PSFs used for deconvolution compared to the PSFs used to simulate the images. Figure 8(a) shows the quadratic error computed between the original image and the deconvolved image as a function of the parameter λ, for a SNR of 3 dB and for increasing angular errors. One can notice that, except for low values of the regularization parameter λ, for which multikernel deconvolution fails to give satisfactory results, the residual error in image reconstruction is always much lower for multikernel deconvolution with kernel misalignments than for monokernel deconvolution, even if slightly higher than for multikernel deconvolution with correct kernels. This is true even for a very large kernel misalignment of 20°.

This a priori surprising result may however be easily explained if one considers the “equivalent”

PSFs, first PSF_{eq} obtained by simply adding, the 4 narrowed PSFs used for acquisition simulations, then $PSF_{eq\text{-}err}$ adding the 4 narrowed PSFs with orientation errors. Figure 8(a) recalls the original narrowed PSF. Figures 8(b) and 8(d) display PSF_{eq} for 2-kernel and 4-kernel deconvolution, respectively. The summation process clearly supports the central regions of each narrowed PSF, which add up, while the extensions are angularly regularly distributed, and as a result, of much lower intensity than the central peak (typically 4 times lower for 4-kernel deconvolution). As a consequence, PSF_{eq} for 4 kernels is almost circular symmetric. Obviously, same conclusion holds for the "equivalent" OTF, which is used in the Thikonov equation (5). When the narrowed PSF used for multikernel deconvolution are by inadvertence rotated, the tails are also rotated, but the central region, where the PSFs sum up, is in fact almost identical. As a consequence, not only is multikernel deconvolution still possible, but furthermore, the high frequency content of this "equivalent" PSF being still enhanced, compared to a regular PSF, better results are obtained with multikernel deconvolution, even with large kernel estimation errors.

Note that for a 2-kernel deconvolution, not only are the results of lower quality than for a 4-kernel deconvolution (see Fig. 5), but it also would be more sensitive to angular rotation errors, as the "equivalent" PSF is not circular symmetric (see Fig. 8(c)).

Interestingly, the lower error obtained for multikernel deconvolution is again possible over a large range over the filtering parameter λ (but narrower than with no error on the kernel), which shows that multikernel deconvolution is robust to simultaneously kernel evaluation errors and the filtering parameter choice.

Again, this result about the robustness to errors in estimation of kernels, obtained in the case of asymmetric PSFs, recalls those obtained by Goudail *et al*. [24] who considered multikernel deconvolution with symmetric PSFs, but of different sizes, and confirms, for confocal fluorescence microscopy, the advantage that multikernel deconvolution with different engineered PSFs would have over averaging deconvolutions performed with a regular PSF, or over multikernel deconvolutions with the same regular PSF.

4. Discussion

We now detail some advantages and drawbacks of our approach, compared to other, more better established, methods to improve the resolution in fluorescence microscopy, and conclude by mentioning some types of fluorescence microscopies, which may benefit from multikernel deconvolution.

4.1 Advantages and drawbacks of the proposed method

In a previous paper, we demonstrated that lateral interfering excitation beams permit to narrow the excitation PSF_{ill} by a factor two in a confocal microscope. This gain is however along one axis only, because of the polarization properties of focalized beams. We have shown that combined with multikernel deconvolution, it is possible to recover an enhanced resolution along both the x- and y-axes.

The axial resolution however is not enhanced with this technique, which is adapted to very shallow specimens. But the lateral interference scheme we consider may be combined with longitudinal interferences appearing when propagating beams passing through two opposing lenses interfere, as in the 4Pi microscope of type A. Figures 9(a) and 9(b) display lateral and longitudinal sections through the confocal PSFs for a regular confocal microscope and a 4Pi type A confocal microscope, respectively. Figure 9(c) shows the excitation PSF_{ill} of a 4Pi type A tribeam microscope, and Fig. 9(d) displays its confocal PSF (all figures are computed for a NA=1.2 water immersion objective, with λ_{ill} = 400 nm and λ_{det} = 500 nm, considering x-polarized excitation beams, and unpolarized detection). Note that the lateral lobes are better suppressed than the longitudinal ones. However, efficient filtering techniques to remove the ghost images due to these remaining longitudinal lobes have already been developed [12]. This result shows that it should be possible to obtain an improved resolution along the z-axis and along the y-axis, simultaneously. Then multiple acquisitions combined with a multikernel deconvolution should permit to obtain the same resolution gain in the third dimension.

We have in fact shown that three-beam excitation confocal microscopy may offer the same lateral resolution than linear structured illumination, which also uses a multiple images acquisition process. Structured illumination has the important advantage that, being a wide-field technique, it induces no loss of photons, which is precious in case of bleaching sensitive dyes. Also, non-linear (saturated) structured illumination has proven to deliver an even better resolution [27]. The method we propose has the drawback of possibly increased bleaching (because of the intense lobes of the excitation PSF_{ill}), but has the advantage that it may be used with two-photon sensitive dyes, which indeed cannot be used with

structured illumination, because the high intensity needed to induce two-photon fluorescence renders the use of focalized beams mandatory. Furthermore, the use of two-photon excitation in fact induces a loss in lateral resolution, because doubling the wavelength imposes a widening of the Airy disk, which is not compensated by the non-linear squaring of the illumination PSF to take into account the two-photon process. As a consequence, our method has the important advantage that it may permit to compensate for this inevitable loss in lateral resolution in two-photon microscopy. In particular, available 4Pi microscopes are currently used in combination with two-photon excitation in order to minimize the secondary longitudinal lobes, and therefore may potentially benefit from our technique.

4.2 Possible extensions of the proposed method

The best results in STED microscopy in terms of resolution have been in fact obtained with an asymmetric PSF, resulting from an excitation PSF depleted by a STED beam presenting a one-direction valley of depletion [28]. With this method, a physical resolution of 40 nm has been obtained, which could even be improved to 28 nm by deconvolution. This spectacular result was however possible along one direction only. If one could obtain with this technique several images of the same specimen, with different orientations of the 1-D valley of depletion, then the method we propose may permit to reconstruct a 2-D specimen with the unsurpassed resolution, which was obtain in 1-D.

Another technique, which may benefit from multikernel deconvolution, is Multiple Imaging Axis Microscopy (MIAM) [29]. Usually, to image large specimen, one has to use low numerical aperture-, long working distance objectives. The images present a bad resolution along the optical axis, because the PSF of such objectives is strongly elongated along this axis, resulting in a marked anisotropy in resolution. In the MIAM approach, 4 such objectives are used in a tetrahedral configuration to image the large fluorescent specimen under 4 different directions. The 4 resulting 3-D images are then recombined (in fact simply summed-up in the original paper [29]), in order to compensate the low resolution along the optical axis of each objective by the good transverse resolution from the three other objectives. This situation is a direct extension in 3-D of the method we propose in this paper for 2-D specimens. The 3-D extension of the multi-kernel algorithm we consider (Eq. (5)) is indeed straightforward.

Similarly, the confocal microscope, even at high NA, suffers from an anisotropic resolution. If one could succeed in obtaining several 3-D images from the same microscopic specimen (for example, using a micro-glass tube like in Ref.[30], but rotating the tube, instead of using 2 imaging devices), multikernel

deconvolution could then permit to reconstruct an improved-, isotropic-resolution 3-D image of this specimen.

Selective Plane Illumination Microscopy [31] is another technique developed to image large specimen with a high resolution. With this technique, numerous images of the same sample are taken using a rotating stage, and recombined in 3-D using Fourier space data fusion. The resolution with a low numerical aperture, long working distance objective is quasi-isotropic, thanks to a sectioning of the detection PSF by a planar sheet of light for illumination. A slight anisotropy may however still remain, depending on the thickness of the light sheet, which is used, and the numerical aperture of the objective. This technique may therefore also benefit from multikernel deconvolution techniques, which would permit to obtain a true isotropic resolution while probably also allow to decrease the number of images to be taken.

Aknowledgements:

The authors gratefully acknowledge Philippe Réfrégier and Bruno Colicchio for enlightening discussions about multi-kernel deconvolution and image restoration techniques.

References

[1] Abbe E., Arch. Mikrosk. Anat. **9** 413 (1873)

[2] D. Minsky, Scanning **10** 128 (1988)

[3] M.G.L. Gustafsson, J. Microsc. **198** 82 (2000)

[4] M.G.L. Gustafsson, Curr. Opin. Struct. Biol. **9** 627 (1999)

[5] B. Bailey *et al.*, Nature **366** 44 (1993)

[6] B. Bailey *et al.*, Proc SPIE **2184** 208 (1994)

[7] V. Krishnamurthi, B. Bailey and F. Lanni, Proc SPIE **2655** 18 (1994)

[8] M. Nagorni and S.W. Hell, J. Opt. Soc. Am. A **18** 49 (2001)

[9] M.G.L. Gustafsson, D.A. Agard and J.W. Sedat, Proc SPIE **2412** 147 (1995)

[10] S.W. Hell and E.H.K. Stelzer, J. Opt. Soc. Am. A **9** 2159 (1992)

[11] M. Nagorni and S.W. Hell, J. Opt. Soc. Am. A **18** 36 (2001)

[12] S.W. Hell, "Increasing the resolution of far-field fluorescence light microscopy by point-spread-function engineering" in *Topics in Fluorescence Spectroscopy; Vol. 5: Nonlinear and Two-Photon-Induced Fluorescence*, J. Lakowicz ed., Plenum Press, New York (1997)

[13] M.G.L Gustafsson, D.A. Agard and J.W. Sedat, US patent 5671085 (1997)

[14] R. Heintzmann and C. Cremer, Proc. SPIE **3568** 185 (1998)

[15] J.T. Frohn, H.F. Knapp, and A. Stemmer, Proc. Natl. Acad. Sci. USA **97** 7232 (2000)

[16] O. Haeberlé and B. Simon, Opt. Comm. **259** 400 (2006)

[17] O. Haeberlé, Opt. Comm. **216** 55 (2003)

[18] P. Török and P. Varga, Appl. Opt. **36** 2305 (1997)

[19] S.F. Gibson and F. Lanni, J. Opt. Soc. Am. A **8** 1601 (1991)

[20] O. Haeberlé *et al.*, Opt. Exp. **11** 2964 (2003)

[21] O. Haeberlé, Opt. Comm. **235** 1 (2004)

[22] B. Richards and E. Wolf, Proc. R. Soc. London Ser. A **253** 358 (1959)

[23] D.C. Ghiglia, J. Opt. Soc. Am. A **1** 398 (1984)

[24] F.Goudail, O.Ruch and P. Réfrégier, Appl. Opt., **39** 6602 (2000)

[25] S.J. Reeves and R.M. Mersereau, Opt. Eng. **29** 446 (1990).

[26] B. Colicchio *et al.*, Opt. Comm. **244** 37 (2005)

[27] M.G.L Gustafsson, Proc. Natl. Acad. Sci. USA **102** 13081 (2005)

[28] W. Wesphal, L. Kastrup and S.W. Hell, Appl. Phys. B, **77** 377 (2003)

[29] J. Swoger, J. Huisken, and E.H.K. Stelzer, Opt. Lett. **28** 1654 (2003)

[30] S. Kikuchi *et al.*, Opt. Comm. **129** 237 (1996)

[31] J. Huisken, J. Swoger, F. Del Bene, J. Wittbrodt and E.H.K. Stelzer, Science **305** 1007 (2004).

Figure Captions

Fig. 1: Scheme to construct interferences between three point spread functions, resulting from three x-polarized beams, and slightly shifted along the y-axis. Both lateral PSFs are dephased by π relatively to the central one. At points M and M', destructive interferences occur, which results in a narrower central PSF.

Fig. 2: (a) Illumination PSF_{ill} for a x-polarized one-beam illumination. (b) corresponding confocal PSF_{conf}. (c) Illumination PSF_{ill} for a three-beam illumination as described in Fig. 1. (d) corresponding confocal PSF_{conf}. The side-lobes are suppressed. For all figures: N.A. = 1.65, λ_{ill} = 400 nm, λ_{det} = 500 nm. The (x-y) arrows are 200 nm long.

Fig. 3: Profiles along the y-axis for: the excitation PSF_{ill} with a three-beam illumination (solid line), the unpolarized detection PSF_{det} (dashed line), and the final confocal PSF_{conf} (dotted line). The lateral lobes of the illumination PSF_{ill} are largely suppressed by confocalization.

Fig. 4: Simulated images with a rotating 3-beam PSF. (a): original numerical object. (b-d): three-beam confocal PSFs from interfering beams linearly polarized at θ=0°, 45° and 90° with respect to the x-axis, respectively. (e-g) corresponding simulated images. (NA=1.2 water immersion objective, with λ_{ill} = 400 nm and λ_{det} = 500 nm).

Fig. 5: Multikernel deconvolution for the same binary object (a) than Figure 4, whose acquisitions have been simulated for (b): n=2 and θ=0° and 90°, (c): n=4 and θ=0°, 45°, 90° and 135°, and finally for (d): n=8 in steps of 22.5°.

Fig. 6: Comparison of multikernel deconvolutions with rotating narrowed PSF at excitation and monokernel deconvolutions with a regular PSF for different SNR: no noise, 20 dB and 3 dB (a): original object. (b)-(d): simulations of acquired images with a three-beam-excitation confocal kernel oriented at

θ=90° with no noise, 20 dB and 3 dB SNR, respectively. (e)-(g): corresponding 4-kernel deconvolutions with no noise, 20 dB and 3 dB SNR. (h)-(i): average of 4 different monokernel deconvolution with no noise, 20 dB and 3 dB SNR.

Fig. 7: Quadratic error curves computed between orignal and reconstructed objects as a function of the regularization parameter λ. Comparison of mono-kernel deconvolution with a regular PSF_{conf} (dashed line) and multikernel (4 kernels) deconvolution combined with a rotating narrowed three-beam PSF_{conf} (solid line). (a): 20 dB SNR, (b): 3 dB SNR. The dashed-line boxes indicate the domain for which multikernel deconvolution performs better than monokernel deconvolution.

Fig. 8: (a): Quadratic error curves computed between orignal and reconstructed objects as a function of the regularization parameter λ and angular error on the kernel estimations, with 3 dB SNR. Thick red curve: monokernel deconvolution. Thick black curve: 4-kernel deconvolution without angular error. Solid line: 5° angular error. Dotted line: 10° angular error. Dashed line: 15° angular error. Dotted-Dashed line: 20° angular error. (b): original narrowed PSF. (c): 2-kernel equivalent PSF. (d): 4-kernel equivalent PSF.

Fig. 9: Application of 3-beam excitation to 4Pi type A microscopy. (a): regular confocal PSF. (b): 4Pi type A confocal PSF. (c) 3-beam-excitation 4Pi illumination. (d) 3-beam-excitation 4Pi type A confocal PSF. (NA = 1.2, λ_{ill}=400 nm, λ_{det}=500 nm).

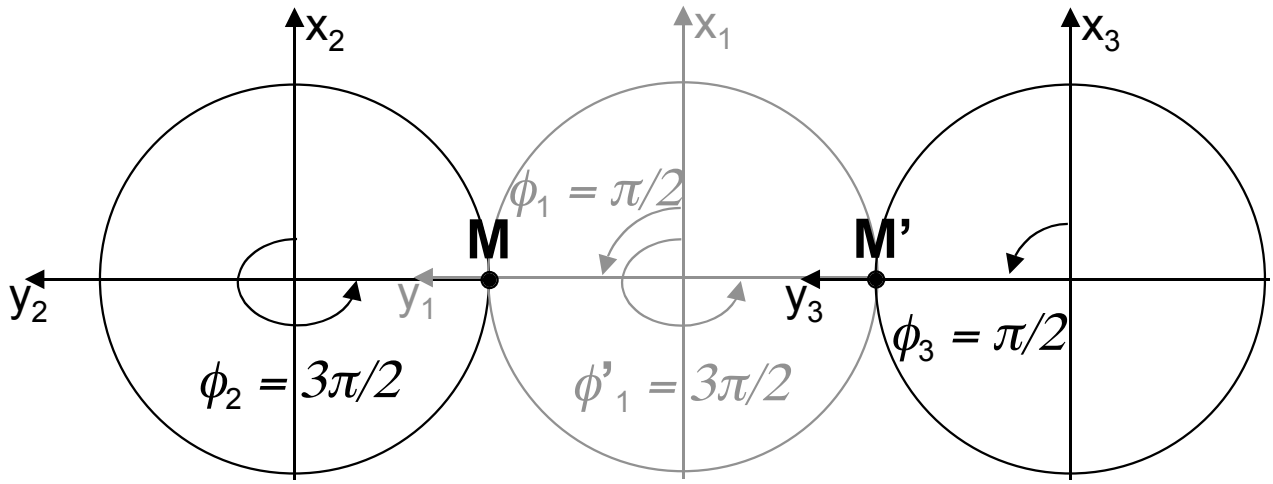

B. Simon and O. Haeberlé, "Multi-kernel deconvolution applied to ……" Figure 1

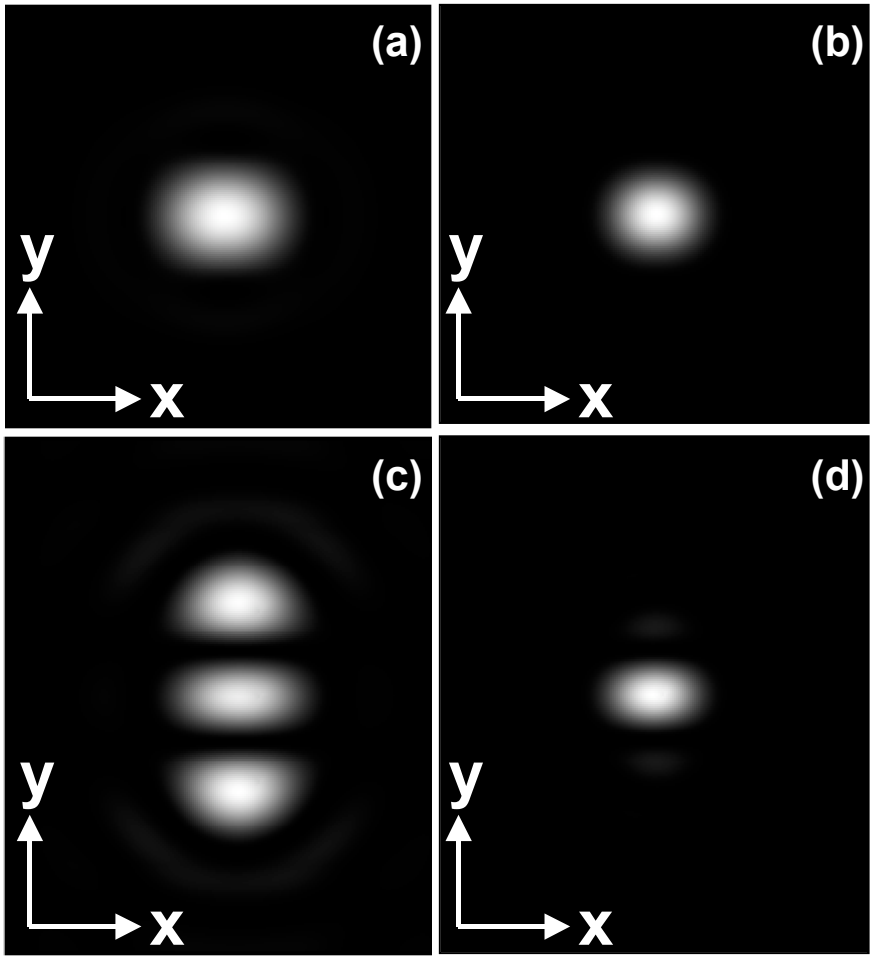

B. Simon and O. Haeberlé, “Multi-kernel deconvolution applied to ……” Figure 2

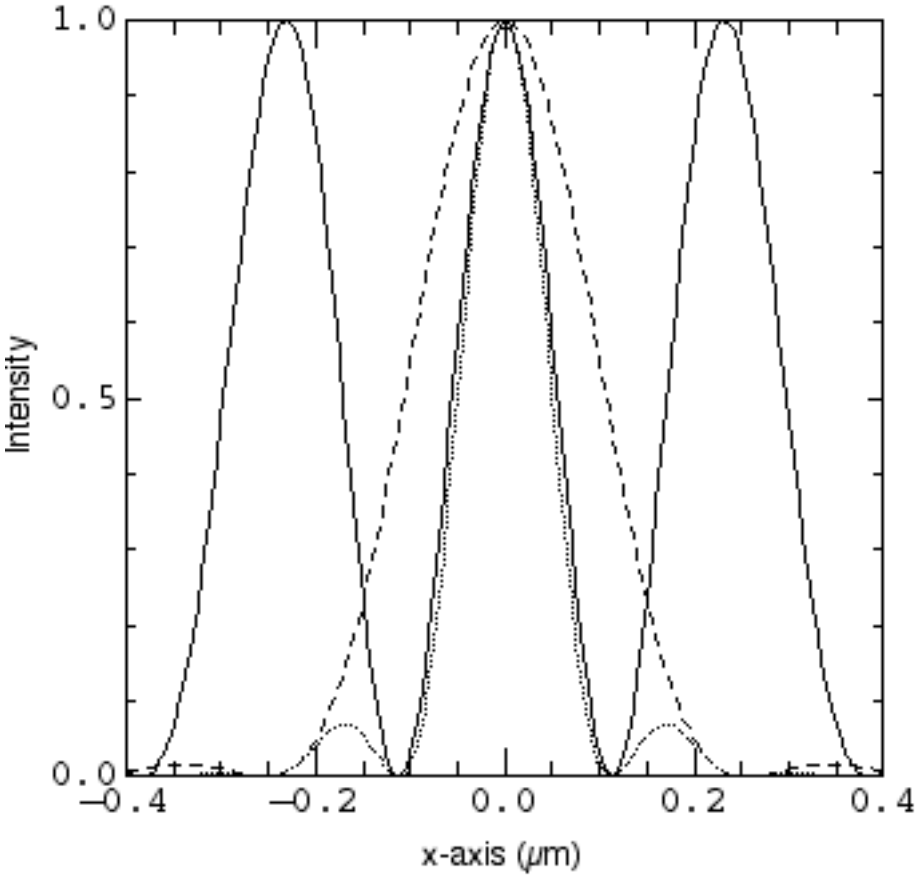

B. Simon and O. Haeberlé, “Multi-kernel deconvolution applied to ……” Figure 3

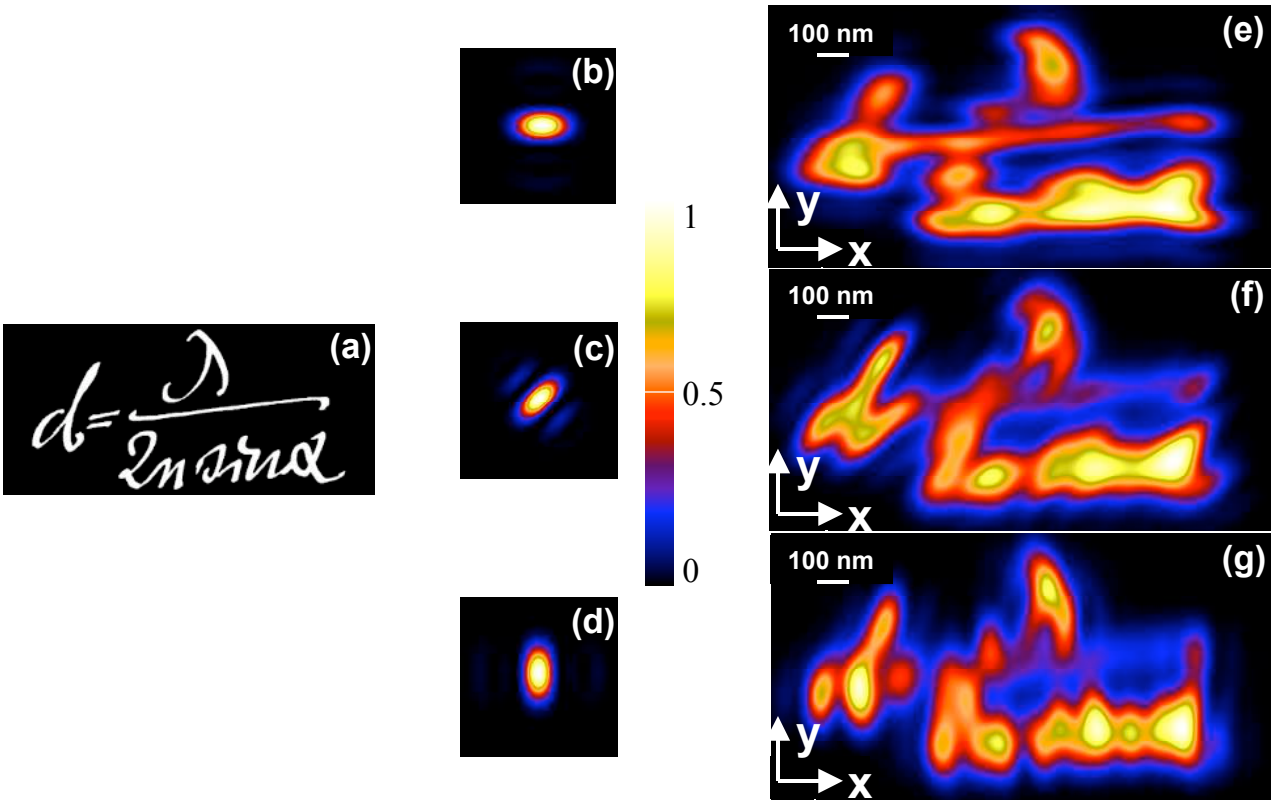

B. Simon and O. Haeberlé, "Multi-kernel deconvolution applied to ……" Figure 4

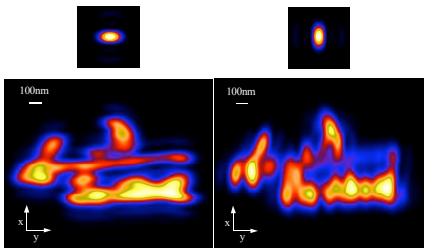

2 kernels (0,90°)

4 kernels (0,45,90,135°)

8 kernels in steps of 22.5°

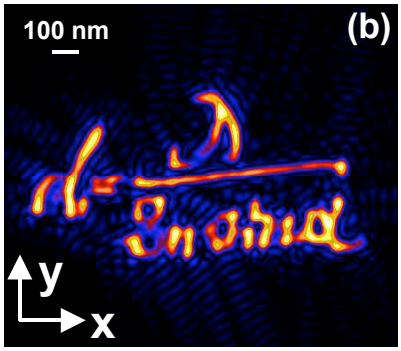

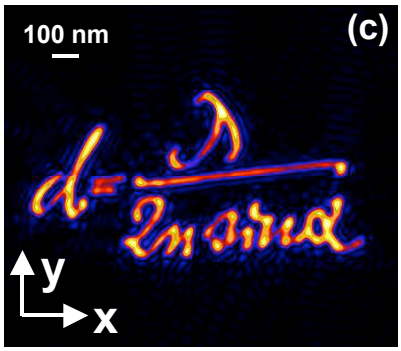

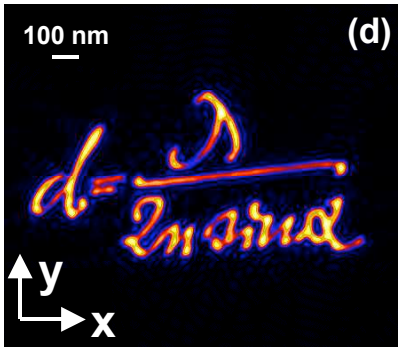

B. Simon and O. Haeberlé, "Multi-kernel deconvolution applied to ……" Figure 5

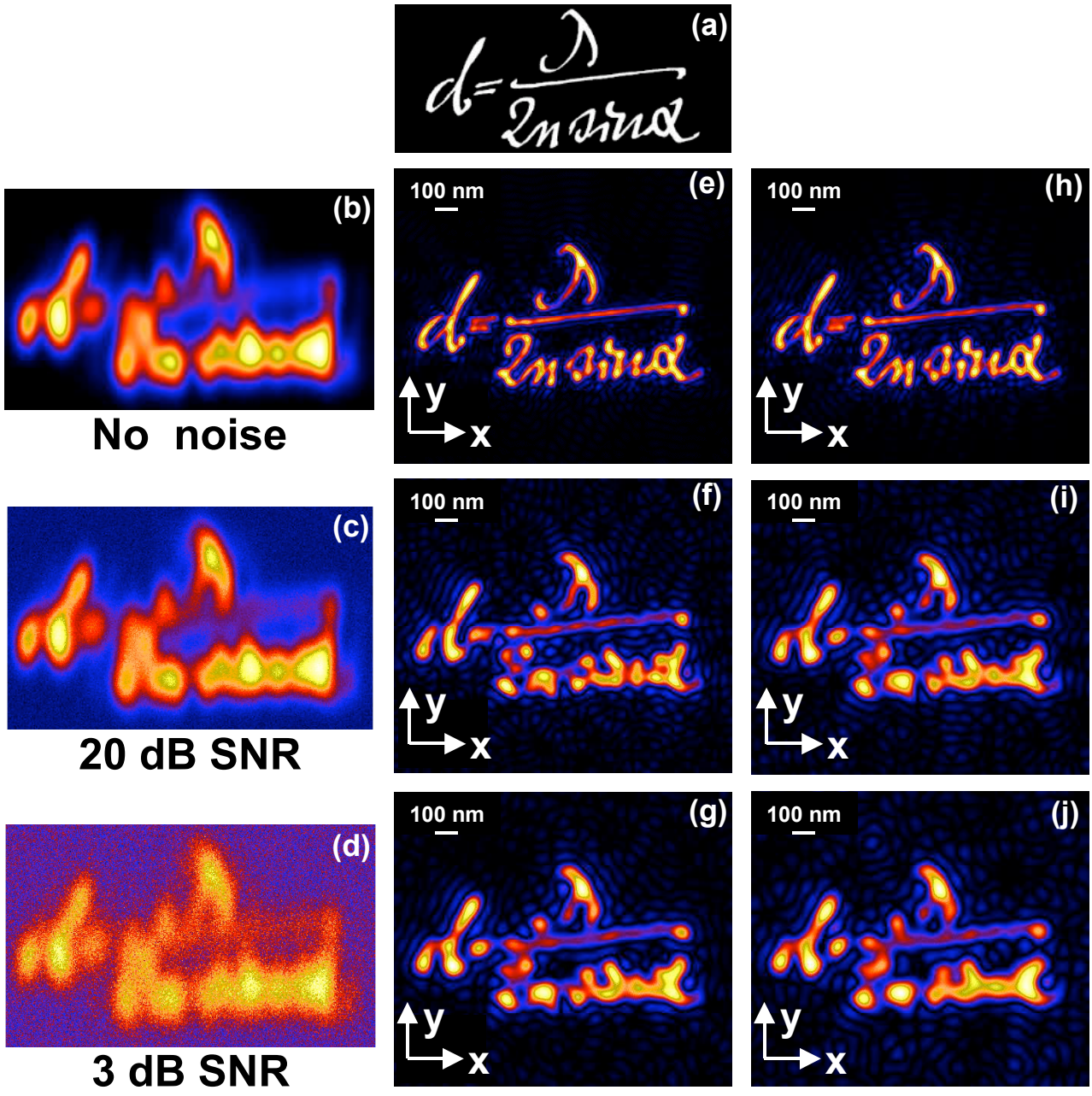

B. Simon and O. Haeberlé, "Multi-kernel deconvolution applied to ……" Figure 6

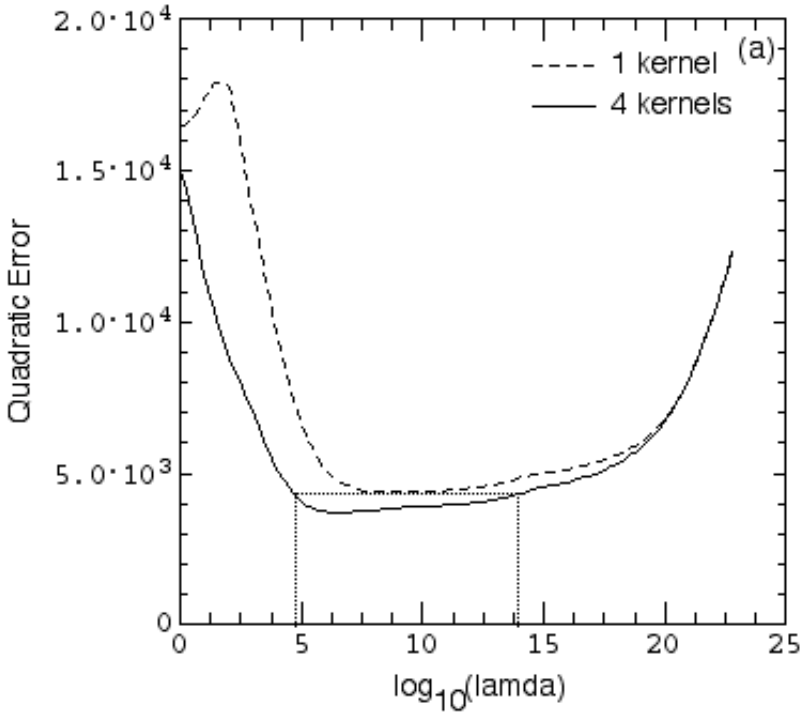

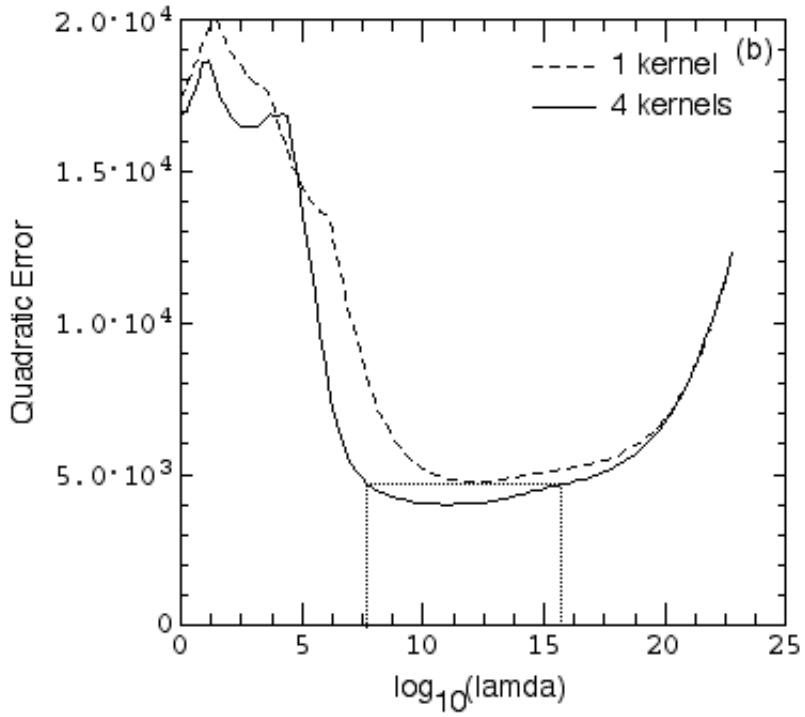

B. Simon and O. Haeberlé, "Multi-kernel deconvolution applied to ……" Figure 7

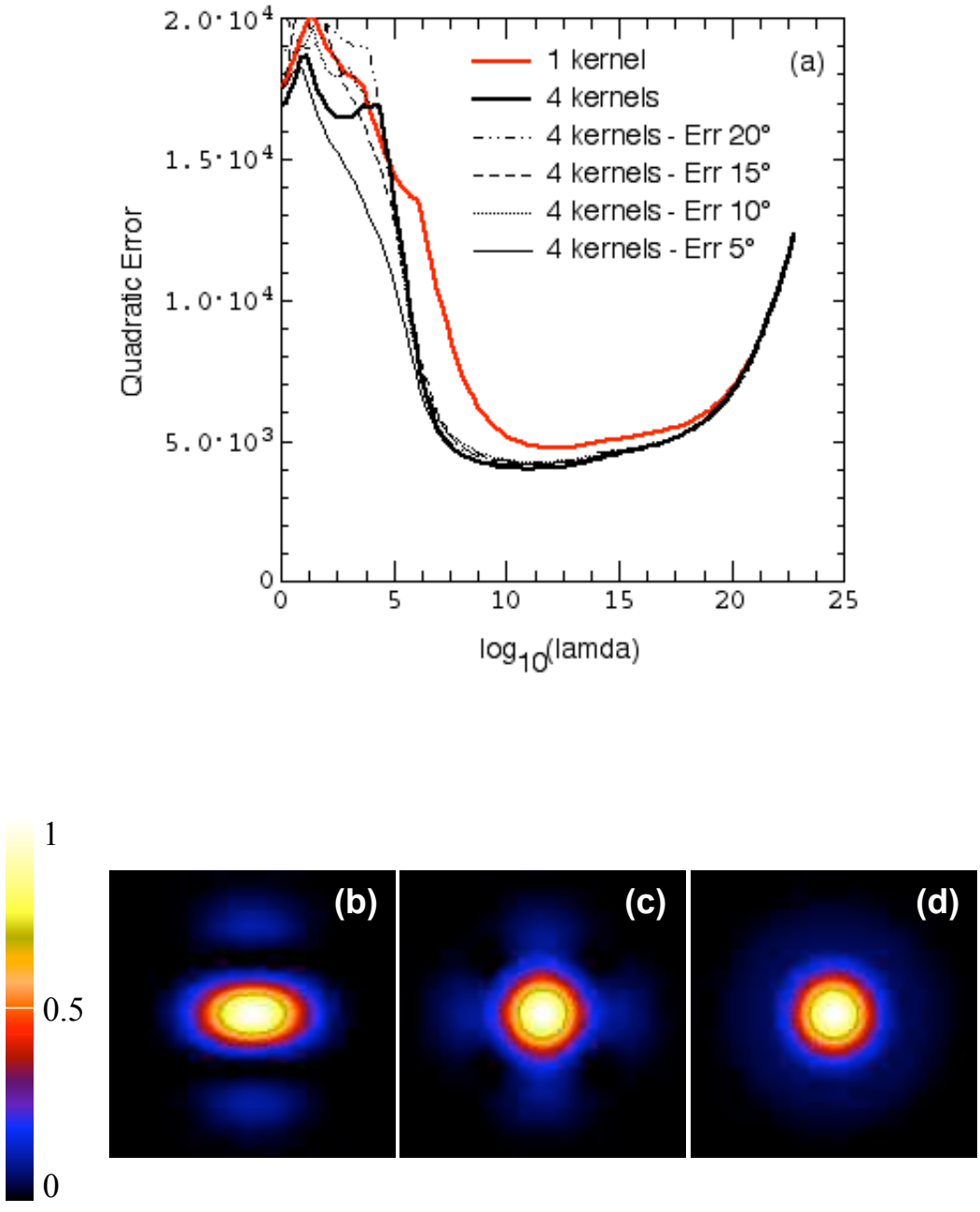

B. Simon and O. Haeberlé, "Multi-kernel deconvolution applied to ……" Figure 8

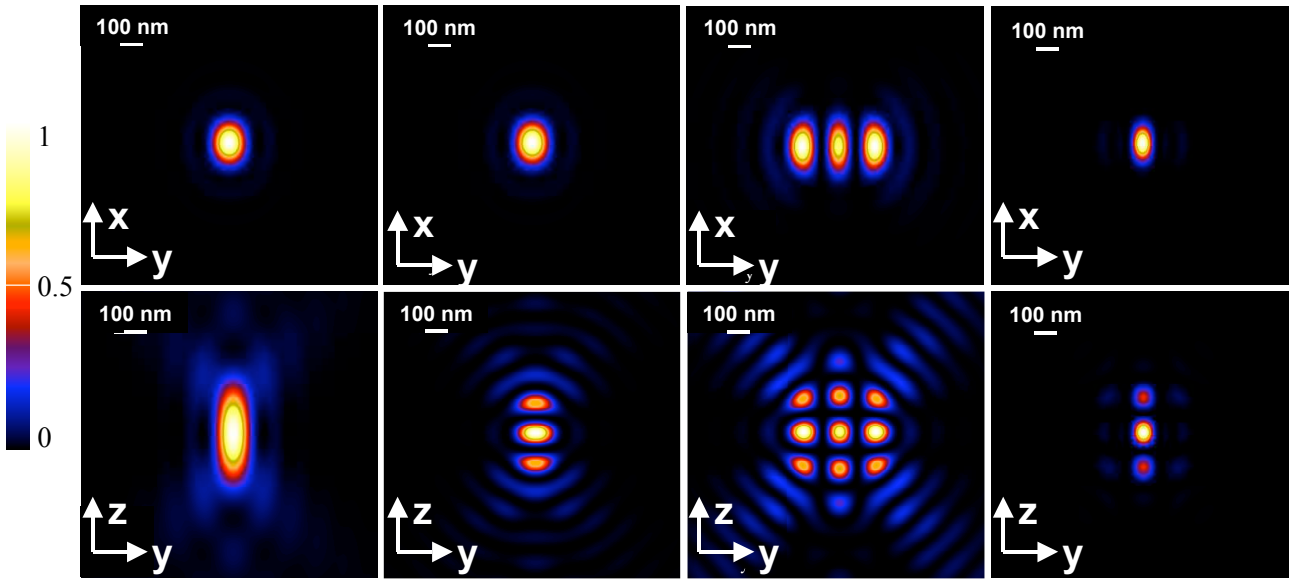

B. Simon and O. Haeberlé, “Multi-kernel deconvolution applied to ……” Figure 9